bioRxiv preprint doi: https://doi.org/10.1101/2022.11.24.516014; this version posted November 25, 2022. The copyright holder for this preprint (which was not certified by peer review) is the author/funder. All rights reserved. No reuse allowed without permission.

Hepatic WDR23 proteostasis mediates insulin clearance by regulating insulin-degrading enzyme activity

Chatrawee Duangjan[1], Thalida Em Arpawong[1], Brett N. Spatola[1], and Sean P. Curran[1,2,*]

1. Leonard Davis School of Gerontology, University of Southern California, Los Angeles, CA 90089
2. Molecular and Computational Biology, Dornsife College of Letters, Arts, and Science, University of Southern California, Los Angeles, CA 90089

*, correspondence to: spcurran@usc.edu

Short title: Loss of *Wdr23* enhances insulin degradation in the liver through IDE

bioRxiv preprint doi: https://doi.org/10.1101/2022.11.24.516014; this version posted November 25, 2022. The copyright holder for this preprint (which was not certified by peer review) is the author/funder. All rights reserved. No reuse allowed without permission.

SUMMARY

Clearance of circulating insulin is critical for metabolic homeostasis. In the liver, insulin is degraded by the activity of the insulin-degrading enzyme (IDE). Here we establish a hepatic regulatory axis for IDE through WDR23-proteostasis. *Wdr23KO* mice have increased IDE expression, reduced circulating insulin, and defective insulin responses. Genetically engineered human cell models lacking *WDR23* also increase IDE expression and display dysregulated phosphorylation of insulin signaling cascade proteins, IRS-1, AKT2, MAPK, and mTOR. Mechanistically, the cytoprotective transcription factor NRF2, a direct target of WDR23-Cul4 proteostasis, mediates the enhanced transcriptional expression of IDE when *WDR23* is ablated. Moreover, an analysis of human genetic variation in *WDR23* across a large naturally aging human cohort in the US Health and Retirement Study reveals a significant association of *WDR23* with altered hemoglobin A1C (HbA1c) levels in older adults that supports the use of WDR23 as new molecular determinant of metabolic health in humans.

KEYWORDS:

Insulin-degrading enzyme (IDE), insulin clearance, WDR23, proteostasis, liver, hepatocytes, NRF2

bioRxiv preprint doi: https://doi.org/10.1101/2022.11.24.516014; this version posted November 25, 2022. The copyright holder for this preprint (which was not certified by peer review) is the author/funder. All rights reserved. No reuse allowed without permission.

INTRODUCTION

The incidence of diabetes continues to increase with over one million new diagnoses each year. Unlike cases of type I diabetes where the individual does not produce an adequate amount of insulin, individuals with type 2 diabetes (T2D) do not effectively respond to the insulin produced. More than 90% of diabetes cases are type 2 and strikingly nearly 90 million new cases of pre-diabetes are documented each year [1, 2]. However, it is estimated that more than 20% of individuals with diabetes are unaware of their condition. Diabetes is diagnosed phenotypically in the clinic, and our understanding of the etiology of T2D and ability to predict a genetic predisposition is currently limited by our understanding of the entirety of molecular regulators that influence this critical metabolic homeostat.

Following its secretion from Beta cells in the pancreas, clearance of endogenously released insulin is primarily achieved by hepatocytes in the liver [3]. Nearly 80% of released insulin is cleared in the first pass through the liver [4] while subsequent passage through the hepatic artery can further deplete insulin from circulation [5]. Defective insulin clearance has been linked to T2D [6] as well as hyperinsulinemia-driven systemic insulin resistance [7, 8] and hyperinsulinemia in metabolic syndrome [9]. In the obese state, hyperinsulinemia results from increased insulin secretion, but also from impaired clearance [10-12].

Insulin-degrading enzyme (IDE) is a ubiquitously expressed metalloprotease with a high affinity for insulin [6, 13]. IDE can degrade insulin in multiple intracellular compartments [14] and genetic ablation of *Ide* results in hyperinsulinemia which suggests IDE plays a central role in insulin clearance. However, non-proteolytic roles for IDE in insulin metabolism by downregulation of the insulin receptor have also been documented [15]. Despite these established roles in insulin metabolism, the regulatory mechanisms that govern IDE expression and activity are not fully understood.

The ubiquitin-proteasome system (UPS) is the primary protein degradation pathway, which plays an important role in cellular proteostasis [16, 17]. Proteins are targeted to the proteasome by a collection of ubiquitin-conjugating enzyme complexes, and poly-ubiquitinated target proteins are degraded by the proteasome [16]. Cullin-RING ligases (CRLs) are a well-known class of E3-ubiquitin ligases found in eukaryotes [17, 18], in which substrate receptors – including DDB1-CUL4 associated factors (DCAFs), also known as WD repeat (WDR) proteins - provide target specificity to the complex. However, the specific substrates for each receptor protein, and their functions in human health and disease, are still largely unknown. Previously, we defined WDR23 as the substrate receptor for the cytoprotective transcription factor NRF2 that functions independently to the canonical KEAP1-CUL3 regulatory pathway [19]. Moreover, GEN1 [17] and SLBP [20] are confirmed substrates of the WDR23-CUL4 proteostat, but additional substrates remain to be identified and are likely to play critical biological functions.

In the present study, we utilize a new *Wdr23KO* mouse model to expand upon our previous investigation of the physiological roles of WDR23, first studied in *C. elegans* [17, 19], and define a role for the WDR23 proteostasis pathway in insulin clearance and organismal metabolic homeostasis. We further define human genetic variation in WDR23 as a factor associated with diabetes. Taken together, our work defines WDR23 as a new factor in cellular and organismal insulin homeostasis.

bioRxiv preprint doi: https://doi.org/10.1101/2022.11.24.516014; this version posted November 25, 2022. The copyright holder for this preprint (which was not certified by peer review) is the author/funder. All rights reserved. No reuse allowed without permission.

RESULTS AND DISCUSSION

Loss of WDR23 disrupts insulin metabolism in male mice

To define the role of WDR23 proteostasis in vertebrate physiology, we commissioned the generation of a floxed allele of *Wdr23* to generate animals lacking *Wdr23* expression in all tissues; hereafter referred to as *Wdr23KO* **(Figure 1A)**. *Wdr23KO* mice are viable, display no overt defects in sexual maturity or reproductive capacity, and display normal body weight in both sexes when compared to wild-type (WT) animals over 44 weeks on a standardized 10% fat diet (**Figure 1B-C,** Figure S1A-B).

We next examined the effect of *Wdr23* deletion on glucose homeostasis and insulin sensitivity by glucose tolerance test (GTT) and insulin tolerance test (ITT), respectively. At all ages tested, male *Wdr23KO* mice display an impairment of insulin sensitivity while exhibiting normal glucose clearance when compared to age-matched WT controls (**Figure 1D-K**). However, the effects of *Wdr23KO* were sexually dimorphic as neither glucose tolerance nor insulin sensitivity were different in female *Wdr23KO* mice as compared to WT (Figure S1C-J). As such, we used male mice in all subsequent experiments.

In light of the potential differences in the responsiveness toward ectopically delivered insulin and the use of endogenously produced insulin [21], we next examined whether steady-state insulin levels were impacted by the loss of *Wdr23*. Surprisingly, we noted a significant reduction in the levels of circulating insulin in *Wdr23KO* mice (**Figure 1L**).

Hepatic steatosis is associated with insulin resistance [21, 22] and as such, we next examined histological comparisons between the livers from 44-week-old mice. We observed no significant changes in liver morphology of *Wdr23KO* mice, compared to the WT mice (Figure S1K-P). Taken together, these data indicated that the loss of *Wdr23* results in early defects in insulin sensitivity; before glucose handling impairment and gross morphological defects in liver organization.

*Wdr23*KO mice accumulate insulin-degrading enzyme (IDE) in the liver

In the ubiquitin proteasome system, loss of a substrate receptor leads to a loss in turnover of substrates associated with that receptor [17, 19, 23, 24]. To identify new substrates of WDR23 we performed an unbiased proteomic analysis of liver from WT and *Wdr23KO* mice. We examined the liver as this tissue plays a crucial role in the regulation of glucose homeostasis [21] and insulin sensitivity [25] and provided adequate sample mass for analysis. 209 unique proteins were identified with increased abundance across the samples; nine (9) proteins were classified as high confidence (>30% change, $p<0.01$) and 200 proteins were classified with moderate confidence (5-30% change, $0.01<p<0.05$) (**Figure 2A;** Table S1). Among the nine high confidence proteins, we found that the level of insulin-degrading enzyme (IDE) was significantly increased in *Wdr23KO* mice liver tissue (**Figure 2A**). IDE is a major enzyme responsible for insulin degradation that plays a central role in hepatic glucose metabolism [26]. As such, the increased levels of IDE could contribute to the insulin resistance phenotype observed. To support this finding, we subsequently confirmed the increased steady-state levels of IDE in fresh liver samples from age-matched WT and *Wdr23KO* mice by western blot analysis (**Figure 2B-D**).

In addition, we assessed IDE proteolytic activity, which was significantly enhanced in liver homogenates from *Wdr23KO* mice as compared to WT (**Figure 2E**). A similar enhancement of IDE enzymatic activity was measured in hepatocytes isolated from *Wdr23KO* mice as compared

bioRxiv preprint doi: https://doi.org/10.1101/2022.11.24.516014; this version posted November 25, 2022. The copyright holder for this preprint (which was not certified by peer review) is the author/funder. All rights reserved. No reuse allowed without permission.

to WT hepatocytes **(**Figure S2A-D**)** suggesting a cellular defect in the major parenchymal cells of the liver [27]. To further confirm specificity of the WDR23-dependent regulation of IDE, we developed a HepG2 cell line where we deleted all copies of *WDR23* by CRISPR/Cas9 genomic editing, hereafter called *WDR23(-/-)* (Figure S2E). As we observed in isolated liver tissues and primary hepatocytes, *WDR23(-/-)* HepG2 cells exhibit an increased level of steady-state IDE expression and enzymatic activity (**Figure 2F-H**, Figure S2F). Importantly, transfection of HepG2 cells with GFP:*WDR23* expression plasmids [17, 19] abolished the increased IDE expression and enhanced enzymatic activity (**Figure 2I-K**, Figure S2G). These data reveal that IDE expression and activity is linked to the insulin metabolism defects in *Wdr23KO* mice.

Loss of Wdr23 drives dysregulated hepatic insulin signaling and glucose handling

An imbalance in insulin signaling can drive metabolic disease due to its activity as a regulator of cellular metabolic homeostasis [28]. This signaling cascade begins with insulin hormones that bind to the insulin receptor (IR), which then trigger the activation of two major kinase-dependent phosphorylation cascades through IRS1/PI3K/AKT and Ras/MAPK pathways [29]. Our unbiased proteomic analyses further revealed significant changes in key downstream mediators of the transcriptional response to insulin signaling that are central to the maintenance of metabolic homeostasis **(**Table S1**).** As such, to directly explore the impact that loss of WDR23-proteostasis plays in the insulin signaling pathway, we next examined the abundance of insulin response pathway proteins whose phosphorylation status mediate the activity of this signaling cascade [28-31].

We first determined the levels of the insulin receptor substrate 1 (IRS-1), which is phosphorylated in response to insulin binding at the insulin receptor. Consistent with the steady-state reduction in insulin levels in liver samples from *Wdr23KO* animals, the phosphorylation of IRS-1 was decreased in *WDR23(-/-)* HepG2 cells compared to control HepG2 cells (**Figure 3A,** Figure S3A). Similarly, AKT2 (**Figure 3B**; Figure S3B) and MAPK (**Figure 3C**, Figure S3C) phosphorylation was significantly decreased in *WDR23(-/-)* HepG2 cells compared to the control HepG2 cells. The PI3K/AKT axis of the insulin signaling cascade regulates metabolic homeostasis through multiple downstream pathways, including the forkhead transcription factor family (FoxO) and the target of rapamycin (mTOR) [28]. We found a modest decrease in the phosphorylation state of mTOR**(Figure 3D;** Figure S3D**)** but no significant change in the phosphorylation state of FoxO1 in *WDR23(-/-)* HepG2 cells (**Figure 3E;** Figure S3E).

Glucose uptake by hepatocytes plays an important role in the liver metabolic homeostat and its response to insulin. To assess whether WDR23 contributes to intracellular glucose influx, we next examined glucose absorption in HepG2 cells with and without *WDR23*. Glucose uptake was significantly decreased in *WDR23(-/-)* HepG2 cells as compared to control HepG2 cells (**Figure 3F**). The major glucose transporter in the plasma membrane of hepatocytes is GLUT2 [32]. We measured the abundance of GLUT2 mRNA (**Figure 3G**) and protein (**Figure 3H,** Figure S3F) which was significantly reduced in *WDR23(-/-)* HepG2 cells and is consistent with the reduced capacity of these cells to transport extracellular glucose. Intriguingly, SLC2A8/GLUT8, which can transport trehalose, a disaccharide consisting of two glucose molecules [33], was identified as ~2-fold upregulated in liver tissues from the *Wdr23*KO mice that may represent a compensatory response to increase carbohydrate influx (Table S4). In addition, the galactose metabolism enzyme GALE was enriched in *Wdr23KO* livers which could aid in the utilization of carbohydrate alternatives to glucose to meet cellular metabolic demands.

bioRxiv preprint doi: https://doi.org/10.1101/2022.11.24.516014; this version posted November 25, 2022. The copyright holder for this preprint (which was not certified by peer review) is the author/funder. All rights reserved. No reuse allowed without permission.

Based on the impaired ability for *WDR23(-/-)* HepG2 cells to transport glucose, we next measured the expression of several key enzymes in the cellular glycolysis and gluconeogenesis pathway. Consistent with a defect in glucose availability, the mRNA expression levels of glucose pathway enzymes including gluconeogenesis pathway genes: Glucose 6-phosphatase (G6Pase), Phosphoenolpyruvate carboxykinase (PEPCK), and Fructose-1,6-bisphosphatase (FBP1); and glycolysis pathway genes: Hexokinase 2 (HK2), Glucose-6-phosphate isomerase (GPI), Fructose-bisphosphate aldolase alpha (ALDOα), glyceraldehyde 3-phosphate dehydrogenase (GAPDH), and Phosphoglycerate kinase 2 (PGK2), were significantly changed in *WDR23(-/-)* samples when compared with WT controls **(Figure 3I)**. Taken together, these data reveal a significant change in the metabolic state of hepatic cells in response to the loss of *Wdr23*.

Loss of *Wdr23* interferes with essential genes in metabolic homeostasis

Based on the altered transcriptional levels of several metabolic homeostasis genes, we next performed next generation RNA-sequencing analyses to discern the scope of transcripts that are sensitive to the activity of the WDR23 proteostasis pathway. Significantly, pathway analysis using the GO and KEGG databases revealed the dysregulated genes induced by *Wdr23* deletion were enriched in carbohydrate metabolic processes that are regulated by insulin signaling and PPAR signaling pathways (Table S2-3**).** These genes are influenced by insulin secretion, insulin resistance, and insulin signaling cascades [28, 34], which were consistent with protein expression results from both isolated liver tissue and HepG2 cells (**Figure 3,** Figure S3, Table S1). We further assessed the differentially expressed genes which revealed enrichment for components of the AGE/RAGE signaling pathway which regulates glucose metabolism in patients with diabetic complications [35] (Table S3)**.** Taken together, the loss of *Wdr23* alters transcription of glucose and insulin metabolism pathways that result in a shift in metabolic homeostasis.

Enhanced expression of IDE is mediated by the WDR23 substrate NRF2

We utilized ChEA3 for transcription factor enrichment analysis by orthogonal -omics integration [36] on our RNAseq data sets to identify transcription factors that mediate the responses to loss of *Wdr23* (Table S4). ChEA3 analysis revealed an enrichment for several transcription factors for the 309 significantly upregulated transcripts, including: CEBPB, which plays a significant role in adipogenesis, as well as in the gluconeogenic pathway; CREB3L3 that plays a crucial role in the regulation of triglyceride metabolism and is required for the maintenance of normal plasma triglyceride concentrations, and NFE2L2/NRF2, which was expected, as our previous work identified NRF2 as a direct target substrate of WDR23 [17, 19]. NRF2 is a conserved cytoprotective transcription factor that controls the expression of stress response and intermediary metabolism gene targets [37-39].

We were curious to test whether the changes in IDE expression and the subsequent insulin metabolism phenotypes in response to loss of *Wdr23* were associated with NRF2 activation. We searched *in silico* within the promoter region of *Ide* for the core ARE-like NRF2 consensus binding sequence [40], 5′-TGAC-3′, and found three putative binding sites for NFE2L2/NRF2 upstream of the translational start site for the human *IDE* locus and six ARE core elements in the mouse genome (**Figure 4A**).

To confirm whether NRF2 is required for the increased expression of IDE in cells lacking *WDR23*, we examined the expression level and activity of IDE in WT and *WDR23(-/-)* HepG2 cells treated with *Nrf2*-specific siRNAs. Following transfection of *NRF2*-specific siRNA, but not transfection with a scrambled siRNA, the enhanced expression of *IDE* transcripts (**Figure 4B**), IDE protein (**Figure 4C**), and the enzymatic activity of IDE (**Figure 4D**) were abrogated. These

bioRxiv preprint doi: https://doi.org/10.1101/2022.11.24.516014; this version posted November 25, 2022. The copyright holder for this preprint (which was not certified by peer review) is the author/funder. All rights reserved. No reuse allowed without permission.

data suggest that NRF2 transcriptional activity largely contributes to the changes in insulin-degrading enzyme when the WDR23 proteostasis pathway is impaired.

Genetic variation in *Wdr23* is associated with the incidence of diabetes in older adults

Based on the remarkable conservation in the players and responses to altered insulin signaling in metabolic health, we were curious if human *WDR23* was associated with metabolic disease states. The US Health and Retirement Study (HRS) is a nationally representative survey of adults aged 50 years and older that is an innovative tool for investigating the normal aging processes [41-43]. Recently, the HRS data sets incorporated genotypic data of participants that enables the testing of associations between normal aging phenotypes and variation across genes [44, 45].

We assessed the available phenotypic data in the US Health and Retirement Study (HRS) for SNP associations with blood-based biomarkers of diabetes and found that genetic variation in *WDR23* is associated with altered hemoglobin A1C (HbA1c) levels. HbA1c is the standard biomarker measure used for the clinical diagnosis of diabetes and pre-diabetes [46]. In HRS, multivariable linear regression models were run to test for the association between each of the five annotated *WDR23* SNPs in the HRS datasets and hemoglobin A1c measurements for each individual **(Figure 4E)**, adjusting for age, gender, and principal components using PLINK. To correct for correlations between SNPs within the gene, we performed 1,000 permutations, comparing shuffled (null) data to the non-shuffled data to derive the empirical p-value threshold of 0.0142 for HbA1c for determining statistically significant associations with *WDR23* SNPs. In the future, as the HRS genotypic data expands and becomes more diverse, an assessment of whether sex and ethnicity are significant drivers of the association of *WDR23* genotype and diabetes will be of great interest. IDE is the major enzyme responsible for insulin degradation in the liver, but also amyloid β (Aβ) regulation in the brain [47].

As such, our collective analyses reveal that *WDR23* genotype influences insulin metabolism and has the potential to impact human health during natural aging. We suggest that *WDR23* can provide an important data point in the development of a personalized medicine approach to ensure optimal health with age.

bioRxiv preprint doi: https://doi.org/10.1101/2022.11.24.516014; this version posted November 25, 2022. The copyright holder for this preprint (which was not certified by peer review) is the author/funder. All rights reserved. No reuse allowed without permission.

ACKNOWLEDGEMENTS

We thank J Gonzalez, M Donoghue, and M Lynn for mouse colony assistance, and Dr. R Irwin, N Stuhr, B Van Camp, and C. Ramos for critical reading of the manuscript. This work was funded by the NIH RF1 AG063947 and R01 AG058610 to SPC and a Glenn Foundation for Medical Research Postdoctoral Fellowship in Aging Research from the American Federation for Aging Research to CD. This study was supported in part by funding from The National Institute on Aging, through the USC-Buck Nathan Shock Center (P30 AG068345). The National Institute on Aging has supported the collection of both survey and genotype data for the Health and Retirement Study through co-operative agreement U01 AG009740. The datasets are produced by the University of Michigan, Ann Arbor. The HRS phenotypic data files are public use datasets, available through: https://hrs.isr.umich.edu/data-products/access-to-public-data. The HRS genotype data are available to authorized researchers: https://www.ncbi.nlm.nih.gov/projects/gap/cgi-bin/study.cgi?study_id=phs000428.v2.p2https://www.ncbi.nlm.nih.gov/projects/gap/cgi-bin/study.cgi?study_id=phs000428.v2.p2. We thank the Wellcome Trust Sanger Institute Mouse Genetics Project (Sanger MGP) and its funders for providing the *Wdr23(tm1a)* mutant mouse line.

AUTHOR CONTRIBUTIONS

Conceptualization, S.P.C.; methodology, T.E.A. and S.P.C.; formal analysis, C.D., B.N.S., T.E.A. and S.P.C.; investigation, C.D., B.N.S., and T.E.A., and S.P.C.; data curation, C.D., B.N.S., T.E.A. and S.P.C.; writing – original draft, C.D. and S.P.C.; writing – review & editing, S.P.C.; visualization, C.D., T.E.A., and S.P.C.; supervision, S.P.C.; project administration, S.P.C.; funding acquisition, C.D. and S.P.C.

DECLARATION OF INTERESTS

The authors declare no competing interests.

bioRxiv preprint doi: https://doi.org/10.1101/2022.11.24.516014; this version posted November 25, 2022. The copyright holder for this preprint (which was not certified by peer review) is the author/funder. All rights reserved. No reuse allowed without permission.

FIGURE LEGENDS

Figure 1. *Wdr23KO* mouse displays impaired insulin homeostasis in males.
Model of Cre-mediated germline deletion of *Wdr23* (**A**). *Wdr23KO* animals gain weight at similar rates as age-matched WT (C57BL/6J) animals (**B,C**). Glucose clearance, as measured by glucose tolerance testing (GTT) is similar between WT and *Wdr23KO* male mice at 10-weeks (**D,E**) and 1-year of age (**F,G**). Insulin tolerance is impaired in *Wdr23KO* male mice fed a standard chow diet (**H, I**) as well as animals fed a chemically defined 10% fat diet (**J, K**).
*p<.05, **p<.01, ***p<.001, ****p<.0001

Figure 2. Loss of *Wdr23* increases insulin-degrading enzyme (IDE) expression and activity in the liver.
(**A**) An unbiased proteomic assessment of proteins in liver from WT and *Wdr23KO* animals reveals an increase in IDE (A), which is confirmed biochemically in freshly isolated livers (**B**). Increased IDE expression is increased at the protein (**C**) and mRNA (**D**) levels that results in enhanced enzymatic activity (**E**) in *Wdr23KO* livers, which is recapitulated in a HepG2 cell line with all copies of *WDR23* deleted "*Wdr23(-/-)*"(**F-H**). Rescue of *WDR23* isoforms suppresses the increased expression of IDE mRNA (**I**) and protein (**J**) and enhanced enzymatic activity (**K**) although IDE mRNA remain high in cells rescued for *WDR23* isoform 2 as compared to WT.
*p<.05, **p<.01, ***p<.001, ****p<.0001

Figure 3. Loss of *WDR23* impairs hepatic insulin pathway signaling
Loss of *WDR23* in HepG2 cells, *WDR23(-/-),* results in diminished insulin signaling pathway activity as measured by a reduction in the phosphorylation state of (**A**) IRS1, (**B**) AKT2, (**C**) MAPK. Correspondingly, a modest reduction in phosphorylation of (**D**) mTOR, but not (**E**) FOXO1 was detected. *Wdr23(-/-)* HepG2 cells have decreased capacity for glucose uptake (**F**) that correlated with reduced abundance of the major glucose transporter of GLUT2 protein (**G**) and mRNA (**H**), and dysregulated expression of glycolytic and gluconeogenic enzymes (**I**).
*p<.05, **p<.01, ***p<.001, ****p<.0001

Figure 4. Enhanced insulin degradation in *Wdr23KO* is mediated by NRF2.
Putative ARE core binding sites in promoter element of the human and mouse *IDE* gene (**A**); numbers are nucleotide position relative to translational start codon (0). The cytoprotective transcription factors NRF2 is necessary for the increased expression of IDE mRNA (**B**), protein (**C**), and insulin degradation enzymatic activity (**D**). HRS data association of *WDR23* variants reveals one variant with significant association with age-related diabetes as measured by HbA1c (**E**). Scan adjusted for age in 2006, sex, and 4 ancestral principal components.
*p<.05; #p<.10 but considered suggestive with multiple test correction set at p=.01.

bioRxiv preprint doi: https://doi.org/10.1101/2022.11.24.516014; this version posted November 25, 2022. The copyright holder for this preprint (which was not certified by peer review) is the author/funder. All rights reserved. No reuse allowed without permission.

STAR METHODS

Key resources table

REAGENT or RESOURCE	SOURCE	IDENTIFIER
Antibodies		
Anti-IRS-1	Cell Signaling	Cat#2382; RRID:AB_330333
Anti-pIRS-1 (Tyr608/Tyr612)	Millipore Sigma	Cat#09-432; RRID:AB_1163457
Anti-AKT2	Cell Signaling	Cat#3063; RRID:AB_2225186
Anti-pAKT2 (Ser474)(D3H2)	Cell Signaling	Cat#8599; RRID:AB_2630347
Anti-MAPK (Erk1/2)	Cell Signaling	Cat#9102; RRID:AB_330744
Anti-pMAPK (Erk1/2)(Thr202/Tyr204)	Cell Signaling	Cat#9101; RRID:AB_2315112
Anti-mTOR	Cell Signaling	Cat#2983; RRID:AB_2105622
Anti-pmTOR(Ser2448)(D9C2)	Cell Signaling	Cat#5536; RRID:AB_10691552
Anti-FoxO1(C29H4)	Cell Signaling	Cat#2880; RRID:AB_2106495
Anti-pFoxO1(Ser256)(E1F7T)	Cell Signaling	Cat#84192; RRID:AB_2800035
Anti-IDE	Millipore Sigma	Cat#AB9210; RRID:AB_2123155
Anti-β actin	Millipore Sigma	Cat#A5441; RRID:AB_476744
Goat anti-Mouse IgG HRP	Thermo Fisher	Cat#31430; RRID:AB_228341
Goat anti-Rabbit IgG HRP	Thermo Fisher	Cat#31460; RRID:AB_228307
Chemicals, peptides, and recombinant proteins		
Fetal Bovine Serum (FBS)	Gibco	Cat#10082147
Minimum Essential Medium	Gibco	Cat#11095-080
Antibiotic/antimycotic	Corning	Cat#30-004-CI
Lipofectamine RNAiMax Reagent	Thermo Fisher	Cat#L3000015
Lipofectamine 3000 Reagent	Thermo Fisher	Cat#13778150
pcDNA 6.2/N-EmGFP/TOPO	Thermo Fisher	Cat#K35920
NRF2 siRNA (s9492)	Thermo Fisher	Cat#4392420
Select negative control No.1 siRNA	Thermo Fisher	Cat#K35920
MTT	AG Scientific	Cat#M-2483
Dimethyl sulfoxide (DMSO)	Sigma Aldrich	Cat#472301
Poly-D-lysine	Sigma Aldrich	Cat#P6407
Mounting medium	Vector Laboratories	Cat#H-1300
Hematoxylin	Sigma Aldrich	Cat#51275
Eosin	Sigma Aldrich	Cat#HT1100216
Glucose	VWR	Cat#BDH9230
Insulin	Humulin R	Cat#0002-8215-17
Tri reagent	Zymo research	Cat#R2050-1-200
M-PER	Thermo Scientific	Cat#78501
Halt protease & phosphatase inhibitor	Thermo Scientific	Cat#78442
Bradford	Sigma Aldrich	Cat#B6916
MOPS running buffer	Invitrogen	Cat#NP001-02
NuPAGE transfer buffer	Invitrogen	Cat#NP00061
BSA	Sigma Aldrich	Cat#A9647-1006
Tween	Bio-Rad	Cat#1610781
Liver perfusion medium	Gibco	Cat#17703-038
Liver digest medium	Gibco	Cat#17703-034

bioRxiv preprint doi: https://doi.org/10.1101/2022.11.24.516014; this version posted November 25, 2022. The copyright holder for this preprint (which was not certified by peer review) is the author/funder. All rights reserved. No reuse allowed without permission.

William's E medium	Gibco	Cat#A1217601
Collagen (type I solution from rat tail)	Sigma Aldrich	Cat#C3867
Primary hepatocyte maintenance supplements	Gibco	Cat#CM4000
Critical commercial assays		
SensoLyte 520 IDE Activity Assay	Ana spec	Cat#AS-72231
Glucose Uptake-Glo Assay	Promega	Cat#J1341
qScript cDNA SuperMix	Quanta Biosciences	Cat#84035
SYBR Green	BioRad	Cat#1725270
Experimental models: Cell lines		
C57BL/6J mouse	Jackson Labs	664
*Wdr23*KO mouse	Wellcome Trust Sanger Institute	N/A
HepG2	Synthego	Synthego SO#4938467-1
HepG2 (*Wdr23-/-*)	This work	N/A
Oligonucleotides		
Mouse *Wdr23* genotyping F:ATGGGATCACGGAACAGCAGC	This work	N/A
Mouse *Wdr23* genotyping R:CTACTGAGGTGAGGAAAAGGCC	This work	N/A
Human *WDR23* genotyping F:CAACCCACCTGGTAAGAGGA	This work	N/A
Human *WDR23* genotyping R: ATGGAAGGGATTGGGGAATA	This work	N/A
qPCR Mouse *Wdr23* F:CTTTCTGCGGCATCTACAGC	This work	N/A
qPCR Mouse *Wdr23* R:TGTAGTCAGACCAGCTGGAGT	This work	N/A
qPCR Human *WDR23* F:AATGACAGAGCTTGGGATGG	This work	N/A
qPCR Human *WDR23* R:GAGGAAAGCTGTGCTTCTGG	This work	N/A
qPCR Mouse *Ide* F:CCACGAGGCTATACGTCCAAG	This work	N/A
qPCR Mouse *Ide* R:ACCATGTCTATCAAGTCGGGTC3	This work	N/A
qPCR Human *Ide* F:CTCTGGAGACTAGACCAAACCA	This work	N/A
qPCR Human *Ide* R:GGGTGTTCAGGAAATTCTGGC	This work	N/A
qPCR Mouse *GAPDH* F:ACAGTCCATGCCATCACTGCC	This work	N/A
qPCR Mouse *GAPDH* R:GCCTGGTTCACCACCTTCTTG	This work	N/A

bioRxiv preprint doi: https://doi.org/10.1101/2022.11.24.516014; this version posted November 25, 2022. The copyright holder for this preprint (which was not certified by peer review) is the author/funder. All rights reserved. No reuse allowed without permission.

qPCR Human *GAPDH* F:TCACCAGGGCTGCTTTTAAC	This work	N/A
qPCR Human *GAPDH* R:GACAAGCTTCCCGTTCTCAG	This work	N/A
qPCR Human *NRF2* F:GTTTGGCTTCTGGAXTTGGA	This work	N/A
qPCR Human NRF2 R:CGGTATGCAACAGGACATTG	This work	N/A
qPCR Human *GCK* F:GCAGAAGGGAACAATGTCGTG	This work	N/A
qPCR Human *GCK* R:CGTAGTAGCAGGAGATCATCGT	This work	N/A
qPCR Human *HK2* F:AAGGCTTCA AGGCATCTG	This work	N/A
qPCR Human *HK2* R:CCACAG GTCATCATAGTTCC	This work	N/A
qPCR Human *GPI* F:CAGAAGCTGCAGCAATGGTA	This work	N/A
qPCR Human *GPI* R:CGTCACCAGGTTCTTGGAGT	This work	N/A
qPCR Human *FBP1* F:TCAACTGCTTCATGCTGGAC	This work	N/A
qPCR Human *FBP1* R:GGGGAACTTCTTCCTCTGGA	This work	N/A
qPCR Human *FBP2* F:CGGGAGATGAGGTGAAGAAA	This work	N/A
qPCR Human *FBP2* R:ATCCATCCAGTGGGTCAAAG	This work	N/A
qPCR Human *ALDOα* F:ATGCCCTACCAATATCCAGCA	This work	N/A
qPCR Human *ALDOα* R:GCTCCCAGTGGACTCATCTG	This work	N/A
qPCR Human *ALDOβ* F:TGTCTGGTGGCATGAGTGAAG	This work	N/A
qPCR Human *ALDOβ* R:GGCCCGTCCATAAGAGAAACTT	This work	N/A
qPCR Human *GAPDH3* F:TCACCAGGGCTGCTTTTAAC	This work	N/A
qPCR Human *GAPDH3* R:GACAAGCTTCCCGTTCTCAG	This work	N/A
qPCR Human *PGK1* F:GACCTAATGTCCAAAGCTGAGAA	This work	N/A
qPCR Human *PGK1* R: CAGCAGGTATGCCAGAAGCC	This work	N/A
qPCR Human *PGK2* F: CACACCGCGCTCATAGTTC	This work	N/A
qPCR Human *PGK2* R:CTCCACCAAGTATAGCCAGAAAG	This work	N/A
qPCR Human *G6Pase* F:CGAGGCGCTACAGAACCAG	This work	N/A

bioRxiv preprint doi: https://doi.org/10.1101/2022.11.24.516014; this version posted November 25, 2022. The copyright holder for this preprint (which was not certified by peer review) is the author/funder. All rights reserved. No reuse allowed without permission.

qPCR Human *G6Pase* R:CACTCGGTGATGAGGCTGAT	This work	N/A
qPCR Human *PEPCK* F:GCAAGATTATCGTCACCC	This work	N/A
qPCR Human *PEPCK* R:GGCATTGAACGCTTTCTCAAAAT	This work	N/A
qPCR Human *G6PC3* F:GCTTCGCCATCGGATTTTAT	This work	N/A
qPCR Human *G6PC3* R:CACCACCTCTGGGCTTTCT	This work	N/A
qPCR Human *ADPGK* F:GCCATGAATATGCTGGAGGT	This work	N/A
qPCR Human *ADPGK* R:ACTGGCCAGCTCTAGGTGAA	This work	N/A
qPCR Human *GLUT1* R:TTGCAGGCTTCTCCAACTGGAC	This work	N/A
qPCR Human *GLUT1* F:CAGAACCAGGAGCACAGTGAAG	This work	N/A
qPCR Human *GLUT2* R:ATGTCAGTGGGACTTGTGCTGC	This work	N/A
qPCR Human *GLUT2* F:AACTCAGCCACCATGAACCAGG	This work	N/A
qPCR Human *GLUT4* R:CCATCCTGATGACTGTGGCTCT	This work	N/A
qPCR Human *GLUT4* F:GCCACGATGAACCAAGGAATGG	This work	N/A
Software and algorithms		
Fiji ImageJ-win64	Fiji	Max Planck Institute of Molecular Cell Biology and Genetics, Dresden Germany
GraphPad Prism 9	GraphPad	https://www.graphpad.com
Other		
Rodent Diet with 10% kcal% fat	Research Diet	Cat#D12450K
4%-12% bis-tris polyacrylamide gel	Invitrogen	Cat#NW04120

Animals

All animal protocols were approved by the Institutional Animal Care and Use Committee (IACUC) of the University of Southern California and all the procedures were conducted in compliance with institutional guidelines and protocols.

Wdr23 knock-out (*Wdr23*KO) mice were generated by Wellcome Trust Sanger Institute [48, 49]. *Wdr23KO* animals were subsequently backcrossed nine times into our C57BL/6J (WT) strain from the Jackson laboratory. Heterozygous (*Wdr23 +/-*) *dams* and *sires* were then mated to generate *Wdr23+/+* and *Wdr23-/-* animals that were maintained as WT and KO, respectively. Male and female mice (n=4-6/group) were kept in a 12:12 h light-dark cycle, constant temperature, and humidity room. All animals were allowed *ad libitum* access to water and food.

Rodent diets

bioRxiv preprint doi: https://doi.org/10.1101/2022.11.24.516014; this version posted November 25, 2022. The copyright holder for this preprint (which was not certified by peer review) is the author/funder. All rights reserved. No reuse allowed without permission.

Mice were fed ad lib with irradiated D12450K rodent chow (Research Diets), containing 16.1kJ/g of digestible energy (animal-based protein 3.22kJ/g, carbohydrate 11.27kJ/g, fat 1.61 kJ/g).

Glucose tolerance tests (GTT)
Performed as previously described [50], Animals (10 weeks and 1 year old) were fasted for 18 h prior to administration of glucose (2g/kg bodyweight) via intraperitoneal injection. Blood glucose was measured from the tail tip at 0, 15, 30, 60-, 90-, 120- and 180-min post-injection (Contour Next One Blood Glucose monitoring (9763).

Insulin tolerance tests (ITT)
Performed as previously described [50]. Animals (30- and 40-weeks old mice) were fasted for 4 hours and then injected intraperitoneally with recombinant human insulin at (0.5 U/kg bodyweight) and glucose levels were determined at 0, 15, 30, 60, 90, 120 and 180 min after insulin injection.

IDE activity assay
The enzymatic activity of IDE in mice liver tissue and HepG2 cells were determined using Sensolyte 520 IDE Activity Assay fluorometric kit according to manufacturer's protocol.

Determination of plasma hormones
Animals were anesthetized, blood samples were taken and centrifuged for 10 min at 10000 rpm, and the supernatant (plasma) was used for hormone measurement. Plasma insulin levels were measured using an ELISA kit (Meso Scale Discovery) according to manufacturer's instructions.

RNA extraction and real-time quantitative PCR
Quantitative PCR was performed as previously described [19]. Briefly, mice liver tissue or HepG2 cells were collected and lysed in Tri reagent (Zymo research,). RNA was extracted according to the manufacturer's protocol. RNA was reverse-transcribed to complementary DNA using qScript cDNA SuperMix (Quanta Biosciences,). Quantitative PCR was conducted by using SYBR Green (BioRad,). The relative expression of each gene was normalized against the internal control gene (GAPDH), and expression levels were analyzed using the 2-ΔΔCT method. The gene-specific sequences of the primers for HepG2 cells and mouse liver tissue were represented in key resources table.

RNA-seq
Isolated RNA was sent to Novogene for library preparation and deep sequencing in biological triplicate. The read counts were used for differential expression (DE) analysis by using the R package DEseq2 (R version 3.5.2). Differentiated expressed genes were analyzed using p value <0.05 and fold change >1.5 as cutoff.

Western blot analysis
Whole cell lysates were prepared in M-PER buffer (1x Mammalian Protein Extraction Reagent (Thermo Scientific,), 0.1% Halt Protease & Phosphatase inhibitor (Thermo Scientific,) according to the manufacturer's protocol. Total protein concentrations were quantified by Bradford assay (Sigma,). An equal amount of protein (20 µg) was separate on 4%-12% bis-tris polyacrylamide gel (Invitrogen,) in MOPS running buffer (Invitrogen,) and then transferred to nitrocellulose membranes (GE Healthcare Life science,). After blocking for 1 h with 3% BSA in PBST (PBS, 0.1% Tween 20), the membranes were subjected to immunoblot analysis. Antibodies used include: IDE (Millipore sigma, 1:5000), IRS-1 (Cell Signaling Technology, 1:500), pIRS-1 (Millipore Sigma, 1:500), AKT (Cell Signaling Technology, 1:1000), pAKT (Cell Signaling Technology, 1:1000), AKT2 (Cell Signaling Technology, 1:1000), pAKT2 (Cell Signaling

bioRxiv preprint doi: https://doi.org/10.1101/2022.11.24.516014; this version posted November 25, 2022. The copyright holder for this preprint (which was not certified by peer review) is the author/funder. All rights reserved. No reuse allowed without permission.

Technology, 1:1000), MAPK (Cell Signaling Technology, 1:1000), pMAPK (Cell Signaling Technology, 1:1000), mTOR (Cell Signaling Technology, 1:1000), pmTOR (Cell Signaling Technology, 1:1000), FoxO1 (Cell Signaling Technology, 1:1000), pFoxO1 (Cell Signaling Technology, 1:1000), β-actin (Millipore Sigma, 1:10000) and HRP-conjugated secondary antibodies (Thermo Fisher, 1:10,000). Specific protein bands were visualized and evaluated using FluorChem HD2 (ProteinSimple). The full images of electrophoretic blots were represented in supplementary materials.

Isolation of mouse primary hepatocytes

Mouse primary hepatocytes were isolated from male *Wdr23*KO and WT mice, aged 3-4 weeks, using a modified collagenase perfusion methods. Briefly, the liver was perfused via the portal vein with perfusion medium (GIBCO) for 6 mins, and liver digest medium (GIBCO) for 5 mins. Liver was removed and placed in a 100 mm plate filled with cold washing medium (William's E medium (WEM, GIBCO), supplemented with GIBCO). Liver was dispersed into small pieces in the medium using forceps and filtered through a 100/70 μM cell strainer into a falcon tube. Cells are collected by centrifugation at 50 g for 3 min and washed 3 times with 20 ml washing medium. The cells were counted, and viability was evaluated by trypan blue exclusion. Hepatocytes were plated in 6 well plates (pre-coated with 0.01% collagen in acetic acid (Sigma) at a density of $2x10^5$ cells per well in maintenance medium (William's E medium (WEM, GIBCO), supplemented with primary hepatocyte maintenance supplements (GIBCO) and incubated for 2-3 hours, 37°C, 5% CO_2.

Cell culture and transfections

WDR23 depleted (*WDR23(-/-)*) HepG2 cells were generated by CRISPR/Cas9 (Synthego). Cells were maintained in Minimum Essential Medium (GIBCO) supplemented with 10% fetal bovine serum (GIBCO) and 1% antibiotic/antimycotic (Corning) at 37°C, 5% CO2.
Full-length cDNA sequence of Hs *WDR23* Isoforms 1 and 2 were cloned into pcDNA 6.2/N-EmGFP/TOPO (Thermo Fisher), as previously described [19]. siRNAs (Thermo Fisher) used include: NRF2 (s9492) and control No.1 (4390843).

Transfections were performed with Lipofectamine 3000 (Thermo Fisher) and Lipofectamine RNAiMAX (Thermo Fisher) according to the manufacturer's protocol.

Glucose uptake measurements

Glucose uptake was performed by using Glucose Uptake-Glo from Promega. Briefly, HepG2 cells were seeded in 96-well plates ($2×10^4$ cells/well) for 24 hours. *WDR23(-/-)* HepG2 cells were transiently transfected with indicated plasmids for 24 hours. Samples were prepared in triplicates for Glucose Uptake-Glo according to manufacturer's protocol, and another setup was for cell viability assay to normalize the cell number.

Cell viability

MTT was used to measure the cell viability. 0.5 mg/ml MTT were added to the culture medium and incubated for 3 h at 37°C. The formazan crystals were solubilized by DMSO.
The absorbance (550) or luminescence were measured using a SPECTRA max M2 Plate Reader. Intracellular glucose uptake was expressed as relative luminescence which normalized by cell viability.

Microscopy

Fluorescence-based imaging

HepG2 cells were grown on coverslips (coated with poly-D-lysine, Sigma) and transiently transfected with *WDR23*-isoform plasmids for 24 hours. The coverslips were mounted (Vector)

bioRxiv preprint doi: https://doi.org/10.1101/2022.11.24.516014; this version posted November 25, 2022. The copyright holder for this preprint (which was not certified by peer review) is the author/funder. All rights reserved. No reuse allowed without permission.

on cover slides and imaged with a Zeiss Axio Imager.M2m microscope, Axio Cam MRm camera and Zen Blue software.

Histological analysis

Liver sections were stained with hematoxylin and eosin (H&E) to visualize adipocytes and inflammatory cells in the tissues. Sections and cells were analyzed by Thunder Imaging Leica DMi8 microscope. H&E-stained sections (six slides for each sample) were randomly selected and quantified for steatosis area using Fiji ImageJ-win64 (Max Planck Institute of Molecular Cell Biology and Genetics, Dresden Germany).

Protein mass spectroscopy

Proteomic characterization of the proteome of mice liver tissues were performed by Poochon Scientific. Briefly, the total protein extractions of tissue samples were prepared following Poochon SOP#602 protocols. The protein concentration of the supernatants was determined by BCA protein assay kit. 90 µg of protein lysate from each sample was run on SDS-PAGE followed by in-gel trypsin digestion, TMT-10plex labeling and LC/MS/MS analysis. The LC/MS/MS analysis was carried out using a Thermo Scientific Q-Exactive hybrid Quadrupole-Orbitrap Mass Spectrometer and Thermo Dionex UltiMate 3000 RSLCnano System. Each peptide fraction was load onto a peptide trap cartridge at a flow rate of 5 µl/min. The trapped peptides were eluted onto a reversed-phase 20 cm C18 PicoFrit column (New Objective, Woburn, MA) using a linear gradient of acetonitrile (3-36%) in 0.1% formic acid, for 100 min at a flow rate of 0.3 µl/min. Then, the eluted peptides from column were ionized and sprayed into the mass spectrometer, using a Nanospray Flex Ion Source ES071 (Thermo) under the following settings: spray voltage, 1.8 kV, capillary temperature, 250 °C. MS Raw data files were searched against the human protein sequence database or other species protein sequence database obtained from NCBI website using the Proteome Discoverer 1.4 software (Thermo, San Jose, CA) based on the SEQUEST and percolator algorithms. The false positive discovery rates (FDR) were set on 1 %. The resulting Proteome Discoverer Report contains all assembled proteins with peptides sequences and peptide spectrum match counts (PSM#) and TMT-tag based quantification ratio. TMT-tag based quantification was used for determining the relative abundance of proteins identified in each set of samples. The calculation and statistical analysis use Microsoft Excel functions. The heat map was generated using R. The annotation including pathways and processes was based on the Kyoto Encyclopedia of Genes and Genomes (KEGG) pathway database and UniProtKB protein database and the NCBI protein database. Samples were normalized to 353 proteins, which were used as control, due to no change between WT and *Wdr23KO* liver samples.

HRS GeneWAS, population stratification, regression models and other covariates, and SNP evaluation

In brief, the US HRS [42, 43, 45] is a nationally representative, longitudinal sample of adults aged 50 years and older, who have been interviewed every 2 years, beginning in 1992. Because the HRS is nationally representative, including households across the country and the surveyed sample now includes over 36,000 participants, it is often used to calculate national prevalence rates for specific conditions for older adults, including physical and mental health outcomes, cognitive outcomes, as well as financial and social indicators. The sample for the current study is comprised of a subset of the HRS for which genetic data were collected, as described below. To reduce potential issues with population stratification, the GeneWAS in this study was limited to individuals of primarily European ancestry. The final sample was N = 3319, with the proportion of women at 58.5%.

HRS *Participants*

bioRxiv preprint doi: https://doi.org/10.1101/2022.11.24.516014; this version posted November 25, 2022. The copyright holder for this preprint (which was not certified by peer review) is the author/funder. All rights reserved. No reuse allowed without permission.

Data are from the *Health and Retirement Study* (HRS), a nationally representative sample of older Americans aged 50 and over [51, 52] in the contiguous United States. The present analysis was limited to participants who self-reported their race as white/Caucasian, verified by principal components analysis of ancestry markers, in order to assess effects of DCAF11 variation found in European ancestry groups. The analytical sample for the HRS included individuals who had available genetic data, at least one measure of hemoglobin A1C data, and relevant covariate data (N=9,326 to 9,333 per SNP based on sample and SNP quality).

DCAF11 Single Nucleotide Polymorphisms (SNPs)

For HRS, genotype data were accessed from the National Center for Biotechnology Information Genotypes and Phenotypes Database (dbGaP [53]). Genotyping was conducted on over 15,000 individuals using either the Illumina HumanOmni2.5-4v1 (2006 and 2008) and HumanOmni2.5-8v1 (2010) arrays and was performed by the NIH Center for Inherited Disease Research (CIDR). Standard quality control procedures were implemented by the University of Washington Genetic Coordinating Center [54]. Further detail is provided in HRS documentation [55]. The DCAF11 SNPs were filtered to include only those with a minor allele frequency of 5% or greater. SNPs were coded in order to assess additive effects of each additional allele (i.e., 0, 1, or 2 minor alleles) and were extracted using PLINK 1.9 [56, 57].

Hemoglobin A1C Biomarkers

The HRS collected biomarkers from blood spots, including glycosylated hemoglobin (HbA1c), which is an indicator of glycemic control over the past 2-3 months. HbA1c was available from blood spots on half of the sample in 2006, and the other half in 2008, with additional individuals captured in the 2010 or 2012 data collection waves. Detailed information on collection and assay are provided elsewhere [58, 59].

Covariates

In HRS, covariates included age at biomarker assessment, gender (0=female, 1=male), and four principal components to reduce such type 1 error due to differences in underlying population substructure [60, 61]. Detailed descriptions of the processes employed for running principal components analysis, including SNP selection, are provided by HRS [55], and follow methods outlined by Patterson and colleagues [62].

Statistical Analysis

In HRS, multivariable linear regression models were run to test for the association between each of the five DCAF11 SNPs and hemoglobin A1C, adjusting for age, gender, and principal components using PLINK. With the number of SNPs and primary phenotypes in this study, strict Bonferroni correction would yield an adjusted multiple test-correction p-value threshold of 0.01 (for 5 SNP tests). However, a Bonferroni correction is too conservative for this type of gene-level assessment because of the correlations between SNPs within the gene [63, 64]. To address this, we calculate empirical p-value thresholds, through permutation procedures [63-66]. Permutation is a process whereby the correlations between SNPs and phenotypes are intentionally shuffled and then p-values calculated for the shuffled (null) data are compared to the non-shuffled data. This procedure is repeated multiple times in order to determine an empirical p-value [64, 66, 67], an empirically derived threshold at which a test result is less likely to achieve significance by chance alone. We performed 1,000 permutations using PLINK to derive the empirical p-value threshold of 0.0142 for HbA1c for determining statistically significant associations with DCAF11 SNPs.

bioRxiv preprint doi: https://doi.org/10.1101/2022.11.24.516014; this version posted November 25, 2022. The copyright holder for this preprint (which was not certified by peer review) is the author/funder. All rights reserved. No reuse allowed without permission.

REFERENCES

1. Saeedi, P., et al., *Global and regional diabetes prevalence estimates for 2019 and projections for 2030 and 2045: Results from the International Diabetes Federation Diabetes Atlas, 9(th) edition.* Diabetes Res Clin Pract, 2019. **157**: p. 107843.
2. Association, A.D., *2. Classification and Diagnosis of Diabetes:.* Diabetes Care, 2021. **44**(Suppl 1): p. S15-S33.
3. Najjar, S.M. and G. Perdomo, *Hepatic Insulin Clearance: Mechanism and Physiology.* Physiology (Bethesda), 2019. **34**(3): p. 198-215.
4. Duckworth, W.C., R.G. Bennett, and F.G. Hamel, *Insulin degradation: progress and potential.* Endocr Rev, 1998. **19**(5): p. 608-24.
5. Tokarz, V.L., P.E. MacDonald, and A. Klip, *The cell biology of systemic insulin function.* J Cell Biol, 2018. **217**(7): p. 2273-2289.
6. BROH-KAHN, R.H. and I.A. MIRSKY, *The inactivation of insulin by tissue extracts; the effect of fasting on the insulinase content of rat liver.* Arch Biochem, 1949. **20**(1): p. 10-4.
7. Corkey, B.E., *Banting lecture 2011: hyperinsulinemia: cause or consequence?* Diabetes, 2012. **61**(1): p. 4-13.
8. Bojsen-Møller, K.N., et al., *Hepatic Insulin Clearance in Regulation of Systemic Insulin Concentrations-Role of Carbohydrate and Energy Availability.* Diabetes, 2018. **67**(11): p. 2129-2136.
9. Pivovarova, O., et al., *Hepatic insulin clearance is closely related to metabolic syndrome components.* Diabetes Care, 2013. **36**(11): p. 3779-85.
10. Shanik, M.H., et al., *Insulin resistance and hyperinsulinemia: is hyperinsulinemia the cart or the horse?* Diabetes Care, 2008. **31 Suppl 2**: p. S262-8.
11. Asare-Bediako, I., et al., *Variability of Directly Measured First-Pass Hepatic Insulin Extraction and Its Association With Insulin Sensitivity and Plasma Insulin.* Diabetes, 2018. **67**(8): p. 1495-1503.
12. Kotronen, A., et al., *Increased liver fat, impaired insulin clearance, and hepatic and adipose tissue insulin resistance in type 2 diabetes.* Gastroenterology, 2008. **135**(1): p. 122-30.
13. Duckworth, W.C., *Insulin degradation: mechanisms, products, and significance.* Endocr Rev, 1988. **9**(3): p. 319-45.
14. Yonezawa, K., et al., *Insulin-degrading enzyme is capable of degrading receptor-bound insulin.* Biochem Biophys Res Commun, 1988. **150**(2): p. 605-14.
15. Villa-Pérez, P., et al., *Liver-specific ablation of insulin-degrading enzyme causes hepatic insulin resistance and glucose intolerance, without affecting insulin clearance in mice.* Metabolism, 2018. **88**: p. 1-11.
16. Callis, J., *The ubiquitination machinery of the ubiquitin system.* Arabidopsis Book, 2014. **12**: p. e0174.
17. Spatola, B.N., et al., *Nuclear and cytoplasmic WDR-23 isoforms mediate differential effects on GEN-1 and SKN-1 substrates.* Sci Rep, 2019. **9**(1): p. 11783.
18. Zimmerman, E.S., B.A. Schulman, and N. Zheng, *Structural assembly of cullin-RING ubiquitin ligase complexes.* Curr Opin Struct Biol, 2010. **20**(6): p. 714-21.
19. Lo, J.Y., B.N. Spatola, and S.P. Curran, *WDR23 regulates NRF2 independently of KEAP1.* PLoS Genet, 2017. **13**(4): p. e1006762.
20. Brodersen, M.M., et al., *CRL4(WDR23)-Mediated SLBP Ubiquitylation Ensures Histone Supply during DNA Replication.* Mol Cell, 2016. **62**(4): p. 627-35.
21. Titchenell, P.M., M.A. Lazar, and M.J. Birnbaum, *Unraveling the Regulation of Hepatic Metabolism by Insulin.* Trends Endocrinol Metab, 2017. **28**(7): p. 497-505.

bioRxiv preprint doi: https://doi.org/10.1101/2022.11.24.516014; this version posted November 25, 2022. The copyright holder for this preprint (which was not certified by peer review) is the author/funder. All rights reserved. No reuse allowed without permission.

22. Shigiyama, F., et al., *Mechanisms of sleep deprivation-induced hepatic steatosis and insulin resistance in mice.* Am J Physiol Endocrinol Metab, 2018. **315**(5): p. E848-e858.
23. Le, R., et al., *Dcaf11 activates Zscan4-mediated alternative telomere lengthening in early embryos and embryonic stem cells.* Cell Stem Cell, 2021. **28**(4): p. 732-747.e9.
24. Xu, Z., et al., *WDR-23 and SKN-1/Nrf2 Coordinate with the BLI-3 Dual Oxidase in Response to Iodide-Triggered Oxidative Stress.* G3 (Bethesda), 2018. **8**(11): p. 3515-3527.
25. Bazotte, R.B., L.G. Silva, and F.P. Schiavon, *Insulin resistance in the liver: deficiency or excess of insulin?* Cell Cycle, 2014. **13**(16): p. 2494-500.
26. Leissring, M.A., *Insulin-Degrading Enzyme: Paradoxes and Possibilities.* Cells, 2021. **10**(9).
27. Zhou, Z., M.J. Xu, and B. Gao, *Hepatocytes: a key cell type for innate immunity.* Cell Mol Immunol, 2016. **13**(3): p. 301-15.
28. Huang, X., et al., *The PI3K/AKT pathway in obesity and type 2 diabetes.* Int J Biol Sci, 2018. **14**(11): p. 1483-1496.
29. Guo, S., *Molecular Basis of Insulin Resistance: The Role of IRS and Foxo1 in the Control of Diabetes Mellitus and Its Complications.* Drug Discov Today Dis Mech, 2013. **10**(1-2): p. e27-e33.
30. Bock, R.E., G.W. Burgess, and I.C. Douglas, *Development of an enzyme linked immunosorbent assay (ELISA) for the detection of bovine serum antibody to bovine viral diarrhoea virus.* Aust Vet J, 1986. **63**(12): p. 406-8.
31. Haeusler, R.A., T.E. McGraw, and D. Accili, *Biochemical and cellular properties of insulin receptor signalling.* Nat Rev Mol Cell Biol, 2018. **19**(1): p. 31-44.
32. Merino, B., et al., *Hepatic insulin-degrading enzyme regulates glucose and insulin homeostasis in diet-induced obese mice.* Metabolism, 2020. **113**: p. 154352.
33. Mayer, A.L., et al., *SLC2A8 (GLUT8) is a mammalian trehalose transporter required for trehalose-induced autophagy.* Sci Rep, 2016. **6**: p. 38586.
34. Lee, S. and H.H. Dong, *FoxO integration of insulin signaling with glucose and lipid metabolism.* J Endocrinol, 2017. **233**(2): p. R67-r79.
35. Kay, A.M., C.L. Simpson, and J.A. Stewart, Jr., *The Role of AGE/RAGE Signaling in Diabetes-Mediated Vascular Calcification.* J Diabetes Res, 2016. **2016**: p. 6809703.
36. Keenan, A.B., et al., *ChEA3: transcription factor enrichment analysis by orthogonal omics integration.* Nucleic Acids Res, 2019. **47**(W1): p. W212-W224.
37. Tebay, L.E., et al., *Mechanisms of activation of the transcription factor Nrf2 by redox stressors, nutrient cues, and energy status and the pathways through which it attenuates degenerative disease.* Free Radic Biol Med, 2015. **88**(Pt B): p. 108-146.
38. Uruno, A., et al., *The Keap1-Nrf2 system prevents onset of diabetes mellitus.* Mol Cell Biol, 2013. **33**(15): p. 2996-3010.
39. Shaw, P. and A. Chattopadhyay, *Nrf2-ARE signaling in cellular protection: Mechanism of action and the regulatory mechanisms.* J Cell Physiol, 2020. **235**(4): p. 3119-3130.
40. Tonelli, C., I.I.C. Chio, and D.A. Tuveson, *Transcriptional Regulation by Nrf2.* Antioxid Redox Signal, 2018. **29**(17): p. 1727-1745.
41. Fisher, G.G. and L.H. Ryan, *Overview of the Health and Retirement Study and Introduction to the Special Issue.* Work Aging Retire, 2018. **4**(1): p. 1-9.
42. Sonnega, A., et al., *Cohort Profile: the Health and Retirement Study (HRS).* Int J Epidemiol, 2014. **43**(2): p. 576-85.
43. Juster, T. and R. Suzman, *An Overview of the Health and Retirement Study*, in *Special Issue on the Health and Retirement Study: Data Quality and Early Results (1995)*. University of Wisconsin Press: The Journal of Human Resources. p. S7-S56.

bioRxiv preprint doi: https://doi.org/10.1101/2022.11.24.516014; this version posted November 25, 2022. The copyright holder for this preprint (which was not certified by peer review) is the author/funder. All rights reserved. No reuse allowed without permission.

44. Liu, Z., et al., *Associations of genetics, behaviors, and life course circumstances with a novel aging and healthspan measure: Evidence from the Health and Retirement Study.* PLoS Med, 2019. **16**(6): p. e1002827.
45. Villa, O., et al., *Genetic variation in.* Elife, 2022. **11**.
46. Lyons, T.J. and A. Basu, *Biomarkers in diabetes: hemoglobin A1c, vascular and tissue markers.* Transl Res, 2012. **159**(4): p. 303-12.
47. Pivovarova, O., et al., *Insulin-degrading enzyme: new therapeutic target for diabetes and Alzheimer's disease?* Ann Med, 2016. **48**(8): p. 614-624.
48. Ryder, E., et al., *Molecular characterization of mutant mouse strains generated from the EUCOMM/KOMP-CSD ES cell resource.* Mamm Genome, 2013. **24**(7-8): p. 286-94.
49. White, J.K., et al., *Genome-wide generation and systematic phenotyping of knockout mice reveals new roles for many genes.* Cell, 2013. **154**(2): p. 452-64.
50. Benedé-Ubieto, R., et al., *Guidelines and Considerations for Metabolic Tolerance Tests in Mice.* Diabetes Metab Syndr Obes, 2020. **13**: p. 439-450.
51. HRS, *Sample Sizes and Response Rates*. 2011, University of Michigan: Ann Arbor, MI. p. 1-13. http://hrsonline.isr.umich.edu/sitedocs/sampleresponse.pdf (Accessed October 12, 2016).
52. Juster, F.T. and R. Suzman, *An overview of the Health and Retirement Study.* Journal of Human Resources, 1995: p. S7-S56.
53. dbGaP, *Health and Retirement Study*. 2012, National Center for Biotechnology Information: Bethesda, MD.
54. Laurie, C.C., et al., *Quality control and quality assurance in genotypic data for genome-wide association studies.* Genetic epidemiology, 2010. **34**(6): p. 591-602.
55. HRS, *Quality control report for genotypic data*. 2012, University of Washington: St. Louis, MO. p. 1-44. http://hrsonline.isr.umich.edu/sitedocs/genetics/HRS_QC_REPORT_MAR2012.pdf (Accessed March 15, 2015).
56. Chang, C.C., et al., *Second-generation PLINK: rising to the challenge of larger and richer datasets.* arXiv preprint arXiv:1410.4803, 2014.
57. Purcell, S., et al., *PLINK: a tool set for whole-genome association and population-based linkage analyses.* American journal of human genetics, 2007. **81**(3): p. 559-75.
58. Crimmins, E., et al., *Documentation of biomarkers in the 2006 and 2008 Health and Retirement Study.* Ann Arbor, MI: Survey Research Center University of Michigan, 2013.
59. Crimmins, E., et al., *Validation of blood-based assays using dried blood spots for use in large population studies.* Biodemography and social biology, 2014. **60**(1): p. 38-48.
60. Tian, C., P.K. Gregersen, and M.F. Seldin, *Accounting for ancestry: population substructure and genome-wide association studies.* Human molecular genetics, 2008. **17**(R2): p. R143-R150.
61. Price, A.L., et al., *Principal components analysis corrects for stratification in genome-wide association studies.* Nature genetics, 2006. **38**(8): p. 904-909.
62. Patterson, N., A.L. Price, and D. Reich, *Population structure and eigenanalysis.* PLoS genetics, 2006. **2**(12): p. e190.
63. Han, B., H.M. Kang, and E. Eskin, *Rapid and accurate multiple testing correction and power estimation for millions of correlated markers.* PLoS Genet, 2009. **5**(4): p. e1000456.
64. Sham, P.C. and S.M. Purcell, *Statistical power and significance testing in large-scale genetic studies.* Nat Rev Genet, 2014. **15**(5): p. 335-46.
65. Dudbridge, F. and A. Gusnanto, *Estimation of significance thresholds for genomewide association scans.* Genet Epidemiol, 2008. **32**(3): p. 227-34.
66. Pahl, R. and H. Schafer, *PERMORY: an LD-exploiting permutation test algorithm for powerful genome-wide association testing.* Bioinformatics, 2010. **26**(17): p. 2093-100.

bioRxiv preprint doi: https://doi.org/10.1101/2022.11.24.516014; this version posted November 25, 2022. The copyright holder for this preprint (which was not certified by peer review) is the author/funder. All rights reserved. No reuse allowed without permission.

67. North, B.V., D. Curtis, and P.C. Sham, *A note on the calculation of empirical P values from Monte Carlo procedures.* Am J Hum Genet, 2002. **71**(2): p. 439-41.

bioRxiv preprint doi: https://doi.org/10.1101/2022.11.24.516014; this version posted November 25, 2022. The copyright holder for this preprint (which was not certified by peer review) is the author/funder. All rights reserved. No reuse allowed without permission.

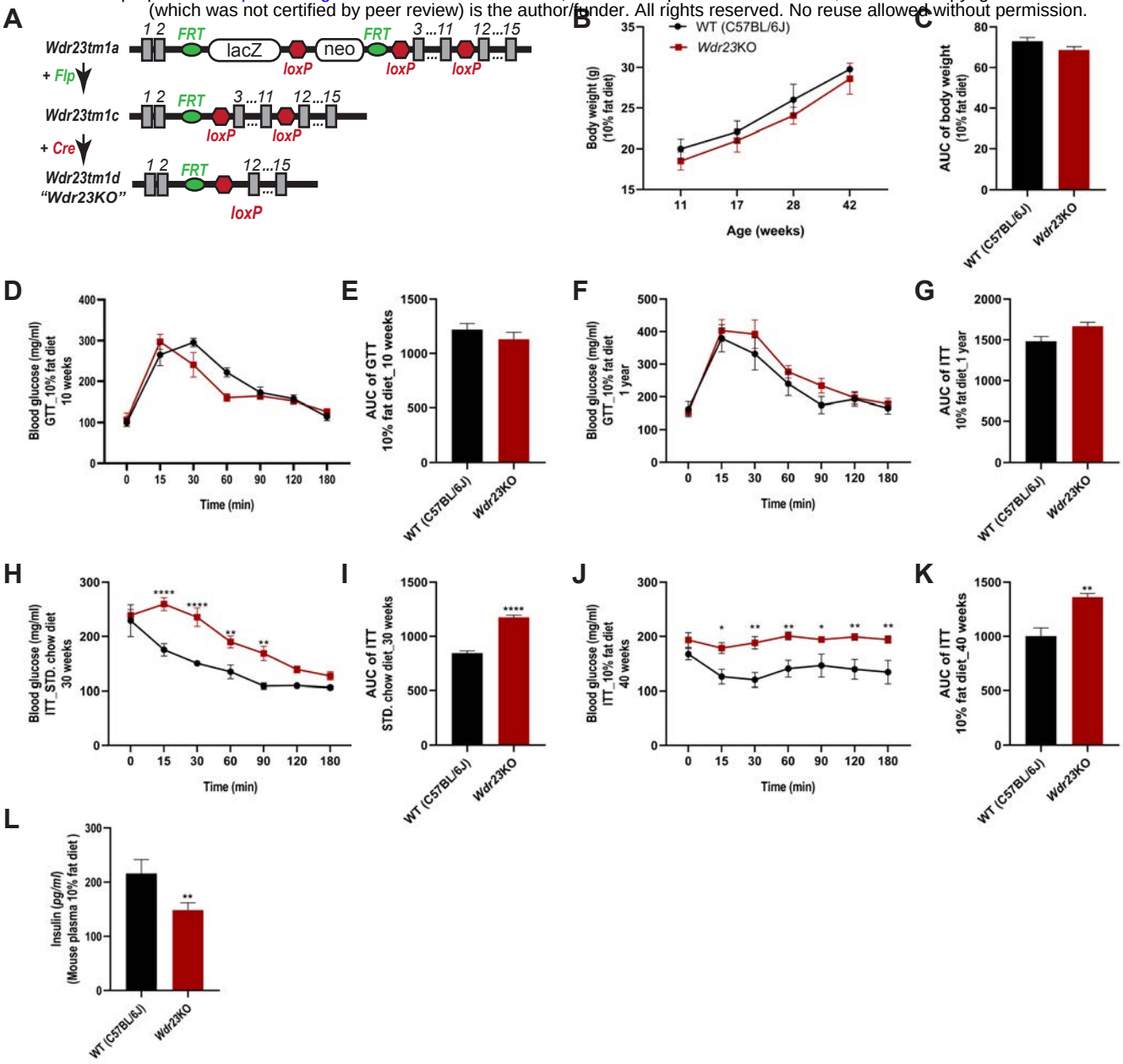

Duangjan Figure 1

bioRxiv preprint doi: https://doi.org/10.1101/2022.11.24.516014; this version posted November 25, 2022. The copyright holder for this preprint (which was not certified by peer review) is the author/funder. All rights reserved. No reuse allowed without permission.

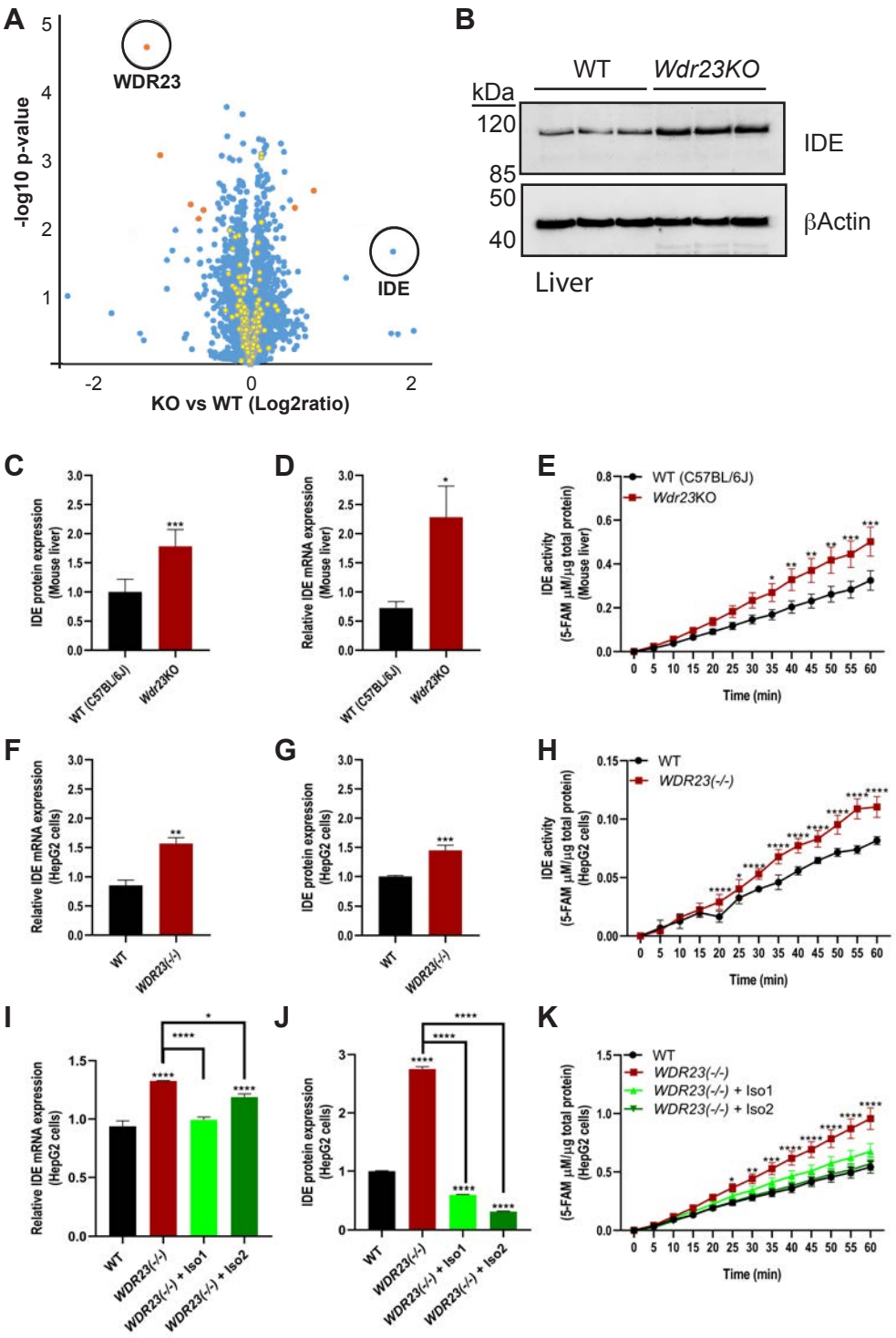

Duangjan Figure 2

bioRxiv preprint doi: https://doi.org/10.1101/2022.11.24.516014; this version posted November 25, 2022. The copyright holder for this preprint (which was not certified by peer review) is the author/funder. All rights reserved. No reuse allowed without permission.

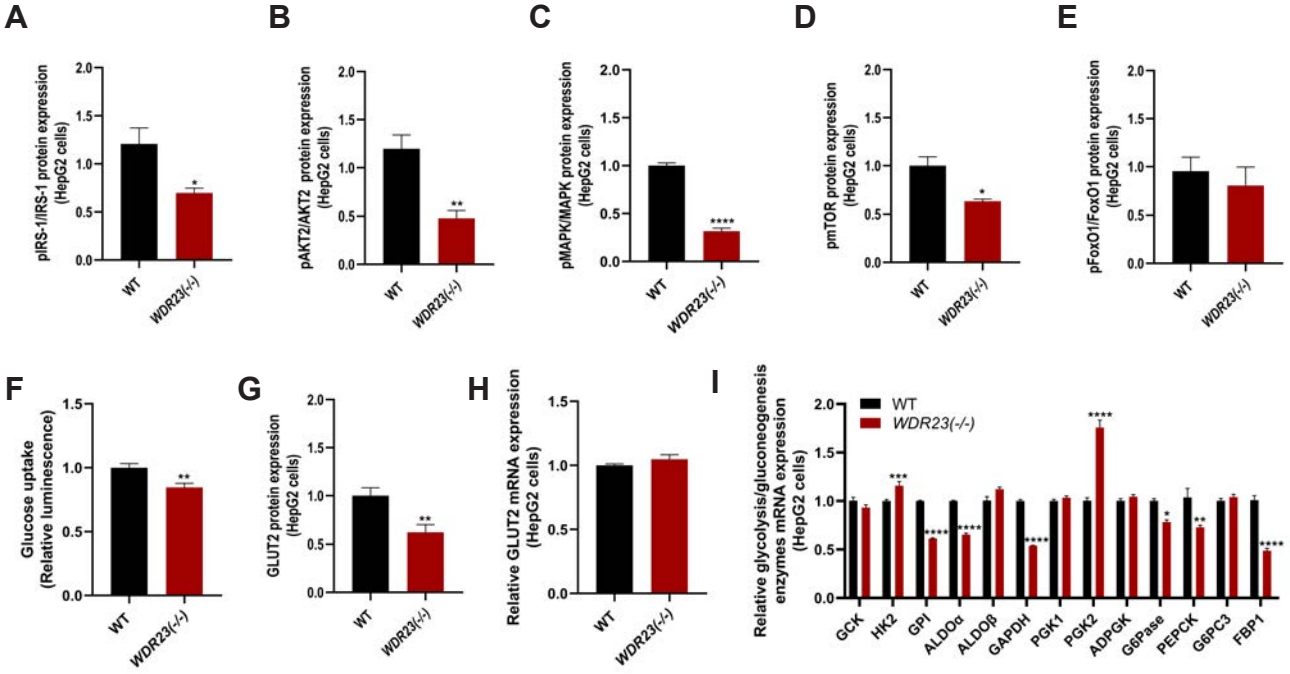

Duangjan Figure 3

bioRxiv preprint doi: https://doi.org/10.1101/2022.11.24.516014; this version posted November 25, 2022. The copyright holder for this preprint (which was not certified by peer review) is the author/funder. All rights reserved. No reuse allowed without permission.

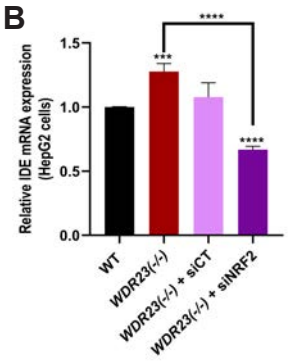

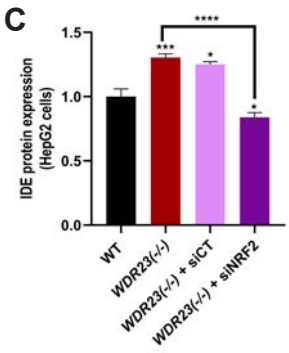

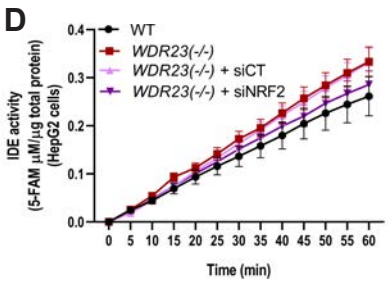

E

SNP	position	Ref allele	NMISS	BETA	P	Significance
rs3742499	24586833	A	9326	-0.015	0.1350	
rs2277481	24587545	G	9331	-0.026	0.0129	*
rs17101367 (kgp6424105)	24587667	A	9328	-0.012	0.2406	
rs2277482	24587795	A	9329	-0.019	0.0670	#
rs2277483	24591892	G	9333	-0.019	0.0650	#

Duangjan Figure 4